Toward a global description of nuclear charge radii: Exploring the Fayans energy density functional

P.-G. Reinhard and W. Nazarewicz

Phys. Rev. C **95**, 064328 — Published 29 June 2017

DOI: 10.1103/PhysRevC.95.064328

Towards the global description of nuclear charge radii: exploring the Fayans energy density functional

P.-G. Reinhard[1] and W. Nazarewicz[2,3]

[1] *Institut für Theoretische Physik II, Universität Erlangen-Nürnberg, D-91058 Erlangen, Germany*
[2] *Department of Physics and Astronomy and FRIB Laboratory, Michigan State University, East Lansing, Michigan 48824, USA*
[3] *Institute of Theoretical Physics, Faculty of Physics, University of Warsaw, Warsaw, Poland*

Background: Binding energies and charge radii are fundamental properties of atomic nuclei. When inspecting their particle-number dependence, both quantities exhibit pronounced odd-even staggering. While the odd-even effect in binding energy can be attributed to nucleonic pairing, the origin of staggering in charge radii is less straightforward to ascertain.

Purpose: In this work, we study the odd-even effect in binding energies and charge radii, and systematic behavior of differential radii, to identify the underlying components of the effective nuclear interaction.

Method: We apply nuclear density functional theory using a family of Fayans and Skyrme energy density functionals fitted to similar datasets but using different optimization protocols. We inspect various correlations between differential charge radii, odd-even staggering in energies and radii, and nuclear matter properties. The Fayans functional is assumed to be in the local FaNDF^0 form. Detailed analysis is carried out for medium-mass and heavy semi-magic nuclei with a particular focus on the Ca chain.

Results: By making the surface and pairing terms dependent on density gradients, the Fayans functional offers the superb simultaneous description of odd-even staggering effects in energies and charge radii. Conversely, when the data on differential radii are added to the pool of fit-observables, the coupling constants determining the strengths of the gradient terms of Fayans functional are increased by orders of magnitude. The Skyrme functional optimized in this work with the generalized Fayans pairing term offers results of similar quality. We quantify these findings by performing correlation analysis based on the statistical linear regression technique. The nuclear matter parameters characterizing Fayans and Skyrme functionals optimized to similar datasets are fairly close.

Conclusion: Fayans paring functional, with its generalized density dependence, significantly improves description of charge radii in odd and even nuclei. Adding differential charge radii to the set of fit-observables in the optimization protocol is helpful for both description of radii and for improving pairing functional. In particular, Fayans functional FaNDF^0 constrained in this way is capable of explaining charge radii in the even-even Ca isotopes. However, in order to obtain good description of differential radii data in both medium-mass and heavy nuclei, an A-dependent scaling of Fayans pairing functional is still needed. Various extensions of the current model are envisioned that carry out a promise for the global description.

I. INTRODUCTION

Charge radii of atomic nuclei are key observables that can probe properties of of nuclear force and nuclear many-body dynamics [1]. They also carry fundamental information about the saturation density of symmetric nuclear matter [2]. The local fluctuations (i.e., rapid changes as a function of particle number) in measured charge radii signal structural evolution effects, such as shell and subshell closures [3], shape deformations [4], and configuration mixing [5]. Another key structural indicator is the odd-even staggering of charge radii along isotopic chains. In particular, the intricate behavior of charge radii along the Ca chain – the almost equal values of charge radii in ^{40}Ca and ^{48}Ca, an appreciable odd-even staggering, and unexpectedly large charge radius in ^{52}Ca [6] – constitute a long-standing challenge for nuclear theory [6–8].

The goal of this study is to understand differential charge radii within nuclear density functional theory (DFT) [9], which is a tool of choice for global microscopic studies of nuclei throughout the chart of nuclides. In nuclear DFT, effective inter-nucleon interaction is represented by the energy density functional (EDF) adjusted to experimental data and often also to selected nuclear matter parameters. While the commonly used energy density functionals offer a very reasonable description of charge radii [10–13] they often miss local fluctuations and dramatically underestimate odd-even effect in radii. In this context, the EDF developed by S.A. Fayans and collaborators [14–18] stands out as it has demonstrated a rare ability to describe charge radii in isotopic chains of semi-magic spherical nuclei, including the challenging Ca chain. A notable achievement of the Fayans model has been to explain the odd-even staggering effect in charge radii in terms of the density-dependent nucleonic pairing [18–21]. In fact, there exist two variants of the Fayans functional, the DF3 functional with finite range couplings [15] and the functional FaNDF^0 involving gradient terms in local couplings [17].

In this work, we carry out detailed analysis of the Fayans energy density functional in FaNDF^0 form, paying attention to its unique features, in particular its density dependence and the role played by surface and pairing gradient terms. We vary the optimization strategies to achieve unbiased comparison of odd-even staggering of

binding energies and charge radii. By means of the statistical covariance technique, we quantify the intricate relation between the pairing functional and charge radii.

This article is organized as follows: Section II contains the description of the models and methods used. In particular, it defines the Fayans functional, datasets employed in various optimization variants, and fitting methodologies employed in this work. The results are contained in Sec. III. Finally, the summary and outlook are given in Sec. IV.

II. THEORETICAL FRAMEWORK

In nuclear DFT, the total binding energy of the nucleus is given by

$$E = \int \mathcal{E}(\boldsymbol{r}) d^3\boldsymbol{r} \tag{1}$$

where $\mathcal{E}$ is the local EDF that is supposed to be a real, scalar, time-even, and isoscalar function of local densities and currents.

A. Local densities

Canonical Hartree-Fock-Bogoliubov (HFB) wave functions and occupation amplitudes uniquely define the one-body density matrix. In this work, we only consider time-reversal-invariant states and thus need only time-even densities. These are [9, 22, 23]: particle density ρ_t, kinetic density τ_t, and spin-orbit current $\boldsymbol{J}_t$, where the isospin index t labels isoscalar ($t = 0$) and isovector ($t = 1$) densities. For instance, the isoscalar and isovector particle densities are:

$$\rho_0 = \rho_n + \rho_p, \quad \rho_1 = \rho_n - \rho_p. \tag{2}$$

If pairing correlations are present, local pairing densities $\breve{\rho}_p$ and $\breve{\rho}_n$ appear as well. In this study, for the purpose of the optimization and statistical analysis, we replace the full HFB problem with the Hartree-Fock (HF)+BCS problem.

B. The Skyrme functional

The Skyrme EDF can be decomposed into the kinetic term, Skyrme interaction term (isoscalar and isovector), pairing EDF, Coulomb term, and additional corrections, such as the center-of-mass (c.m.) term [9, 12, 24]. The Skyrme interaction EDF is $\mathcal{E}_{\rm Sk} = \mathcal{E}_{\rm Sk,0} + \mathcal{E}_{\rm Sk,1}$, where

$$\begin{aligned}\mathcal{E}_{{\rm Sk},t} = {} & C_t^{\rho\rho}(\rho_0)\rho_t^2 + C_t^{\rho\tau}\rho_t\tau_t + C_t^{\rho\Delta\rho}\rho_t\Delta\rho_t \\ & + C_t^{\rho\nabla J}\rho_t\nabla\cdot\boldsymbol{J}_t + C_t^{J^2}\boldsymbol{J}_t^2,\end{aligned} \tag{3}$$

with the coupling constants $C_t^{\rho\rho}$ containing an additional dependence on the isoscalar density:

$$C_t^{\rho\rho}(\rho_0) = C_{t0}^{\rho\rho} + C_{t{\rm D}}^{\rho\rho}\rho_0^{\alpha}. \tag{4}$$

The tensor spin-orbit terms $\propto \boldsymbol{J}_t^2$ are neglected here, i.e., we assume $C_t^{J^2} = 0$.

In this study, the Coulomb Hartree term is calculated exactly using the proton density ρ_p:

$$E_{\rm C} = e^2 \int d^3r\, d^3r' \rho_p(\boldsymbol{r}) \frac{1}{|\boldsymbol{r}-\boldsymbol{r}'|} \rho_p(\boldsymbol{r}'). \tag{5}$$

The exchange term is computed within the standard Slater approximation:

$$\mathcal{E}_{\rm C,ex} = -\tfrac{3}{4}e^2 \left(\frac{3}{\pi}\right)^{1/3} \rho_p^{4/3}. \tag{6}$$

The c.m. correction $E_{\rm cm} = -\langle \hat{P}_{\rm cm}^2 \rangle/(2mA)$ is added to the total energy after the mean-field equations have been solved. The pairing EDF is described by the density-dependent pairing term $\mathcal{E}_{\rm pair} = \mathcal{E}_{{\rm pair},p} + \mathcal{E}_{{\rm pair},n}$ [25, 26]:

$$\mathcal{E}_{{\rm pair},q} = \frac{1}{4} V_{{\rm pair},q} \left(1 - \frac{\rho_0}{\rho_{\rm pair}}\right) \breve{\rho}_q^2 \qquad (q = p, n). \tag{7}$$

We note that the pairing EDF in the Skyrme model has in general different coupling constants for protons and neutrons, see discussion in Ref. [27]. In the limit of $\rho_{\rm pair} \to \infty$, Eq. (7) represents volume pairing and $\rho_{\rm pair} = 0.16\,{\rm fm}^{-3}$ corresponds to what is called surface pairing. The functional SV-min [24] has a mixed pairing with $\rho_{\rm pair} = 0.21159\,{\rm fm}^{-3}$.

C. The Fayans functional

Compared to the Skyrme functional, Fayans FaNDF^0 [17, 28], DF3 [15, 18, 29, 30], and DF3-a [31] EDFs have a more complex dependence on particle densities that stems from a fractional form of their density-dependent couplings, novel folding/density-gradient terms, and Coulomb-nuclear correlation term. The kinetic energy and Coulomb Hartree terms of Fayans EDF are exactly the same as in the Skyrme model. The Fayans interaction functional is usually written in terms of dimensionless densities

$$x_t = \frac{\rho_t}{\rho_{\rm sat}}, \quad x_{\rm pair} = \frac{\rho_0}{\rho_{\rm pair}}, \tag{8}$$

where $\rho_{\rm sat}$ and $\rho_{\rm pair}$ are scaling parameters of Fayans EDF. In the Fayans model, $\rho_{\rm sat}$ is interpreted as the saturation density of symmetric nuclear matter with Fermi energy $\varepsilon_F = (9\pi/8)^{2/3}\hbar^2/2mr_s^2$ and the Wigner-Seitz radius $r_s = (3/4\pi\rho_{\rm sat})^{1/3}$. Note that we have to distinguish between the parameter $\rho_{\rm sat}$, which is an input to the model and the equilibrium density $\rho_{\rm eq}$, which is result of optimization and characterizes Fayans EDF. While these two quantities are close, they are not identical.

In this work, we study Fayans functional in the form of FaNDF^0 as its surface energy is directly expressed through local densities. However, we re-optimize its parameters under various conditions. Thus we distinguish

between the "FaNDF^0 functional" and the "FaNDF^0 parametrization," where the latter is the FaNDF^0 functional with the original model parameters of Ref. [17]. The FaNDF^0 EDF can be decomposed into volume, surface, and spin-orbit terms,

$$\mathcal{E}_{\rm Fy} = \mathcal{E}^{\rm v}_{\rm Fy}(\rho) + \mathcal{E}^{\rm s}_{\rm Fy}(\rho) + \mathcal{E}^{\rm ls}_{\rm Fy}(\rho, \boldsymbol{J}). \tag{9}$$

The volume term $\mathcal{E}^{\rm v}_{\rm Fy}$ is defined as Padé approximant:

$$\mathcal{E}^{\rm v}_{\rm Fy} = \tfrac{1}{3}\varepsilon_F\rho_{\rm sat}\left[a^{\rm v}_+\frac{1-h^{\rm v}_{1+}x_0^\sigma}{1+h^{\rm v}_{2+}x_0^\sigma}x_0^2 + a^{\rm v}_-\frac{1-h^{\rm v}_{1-}x_0}{1+h^{\rm v}_{2-}x_0}x_1^2.\right] \tag{10}$$

Such density dependence in the volume term had also been studied in the context of Skyrme EDF's [32] and found to make not much difference as compared to the form (4). The important new aspect is that the surface term $\mathcal{E}^{\rm s}_{\rm Fy}$ has also the form of a Padé approximant involving the gradient of density:

$$\mathcal{E}^{\rm s}_{\rm Fy} = \tfrac{1}{3}\varepsilon_F\rho_{\rm sat}\frac{a^{\rm s}_+ r_s^2(\nabla x_0)^2}{1 + h^{\rm s}_+x_0^\sigma + h^{\rm s}_\nabla r_s^2(\nabla x_0)^2}. \tag{11}$$

Similar as in the Skyrme case [33, 34], the spin-orbit term $\mathcal{E}^{\rm ls}_{\rm Fy}$ of Fayans functional is derived from zero-range two-body spin-orbit and tensor interactions [29–31, 35, 36]. For time-even spherical nuclei, it can be written as:

$$\mathcal{E}^{\rm ls}_{\rm Fy} = \frac{4\varepsilon_F r_s^2}{3\rho_{\rm sat}}\left(\kappa\rho_0\nabla\cdot\boldsymbol{J}_0 + \kappa'\rho_1\nabla\cdot\boldsymbol{J}_1 + g\boldsymbol{J}_0^2 + g'\boldsymbol{J}_1^2\right). \tag{12}$$

Again, we ignore here the tensor contributions ($g = g' = 0$) as in the original FaNDF^0. The remaining term is identical to that of the Skyrme functional (3) if one identifies $C_0^{\rho\nabla J} = \frac{4\varepsilon_F r_s^2}{3\rho_{\rm sat}}\kappa$ and $C_1^{\rho\nabla J} = \frac{4\varepsilon_F r_s^2}{3\rho_{\rm sat}}\kappa'$.

The Coulomb exchange energy of Fayans functional contains an additional Coulomb-nuclear correlation term:

$$\mathcal{E}_{\rm C,ex} = -\tfrac{3}{4}e^2\left(\frac{3}{\pi}\right)^{1/3}\rho_p^{4/3}(1 - h_{\rm C}x_0^\sigma). \tag{13}$$

Finally, the pairing functional of the Fayans model goes beyond the density-dependent ansatz (7):

$$\mathcal{E}^{\rm pair}_{{\rm Fy},q} = \tfrac{2\varepsilon_F}{3\rho_{\rm sat}}\breve{\rho}_q^2\left[f^\xi_{\rm ex} + h^\xi_+x^\gamma_{\rm pair} + h^\xi_\nabla r_s^2(\nabla x_{\rm pair})^2\right]. \tag{14}$$

This pairing functional is supposed to effectively account for the coupling to surface vibrations; it has a surface character and contains the novel density-gradient term, which is essential for explaining the odd-even staggering in $r_{\rm ch}$ [18, 20].

Following the original FaNDF^0 definitions [17], we use $\hbar^2/2m_p = 20.749811\,\text{MeV fm}^2$, $\hbar^2/2m_n = 20.721249\,\text{MeV fm}^2$, $e^2 = 1.43996448\,\text{MeV fm}$, $\rho_{\rm sat} = 0.16\,\text{fm}^{-3}$, and $\sigma = 1/3$. As in Ref. [17], we also take $\rho_{\rm pair} = \rho_{\rm sat}$. In the FaNDF^0 parametrization, the surface-energy parameter $h^{\rm s}_+$ was assumed to be equal to $h^{\rm v}_{2+}$. Initially, we released this condition and kept it as a free parameter. It turned out, however, that the $h^{\rm s}_+$ is poorly constrained by our datasets, i.e., the associated uncertainties are large. We found that the value $h^{\rm s}_+ = 0$ yields more robust fits than the standard FaNDF^0 value, and we adopted it in our work. For the same reason, since the Coulomb-nuclear correlation term hardly impacts the optimization results, we put $h_{\rm C} = 0$. Finally, we took the exponent $\gamma = 2/3$ in (14) as in DF3-a as it has been shown advantageous for reproducing differential radii [8, 18, 37]. The c.m. correction has been ignored in the original Fayans model. We include it in this work for the sake of comparison with Skyrme results (except for the original FaNDF^0 parametrization); this correction is of minor importance for the quantities discussed here.

D. Mixed Skyrme/Fayans functional

Skyrme EDF and FaNDF^0 EDF differ in two respects. First, the mean-field part has a different density dependence, particularly in the surface term (11), and second, the FaNDF^0 pairing functional has a gradient term, which is absent in the Skyrme model. Changing two features at once can blur comparisons. Thus we also consider as intermediate step a mixed functional, which takes the mean field part from Skyrme EDF and pairing part from FaNDF^0 EDF. We refer to such a mixed functional as "Sk+PFy". The mixed functional helps in two ways. Comparing Skyrme EDF with Sk+PFy explores the Fayans pairing functional, while comparing Sk+PFy with full FaNDF^0 EDF highlights the role of the gradient term in Fayans surface functional.

E. Observables studied

The basic observables calculated in DFT are binding energy $E_{\rm B}$ and local particle densities ρ_t. The charge density $\rho_{\rm ch}$ can be directly obtained from ρ_p and ρ_n by correcting for proton and neutron form factors, and the spin-orbit contribution. The key parameters of the charge density are r.m.s. charge radius $r_{\rm ch}$, diffraction (or box-equivalent) radius $R_{\rm diff}$, and surface thickness $\sigma_{\rm ch}$ [38]. In the following, we shall study isotopic trends of binding energy and charge radii. In particular, we are going to investigate differential mean-square (ms) charge radii, which, for a given isotope, are defined as:

$$\delta\langle r^2\rangle^{A,A'} = \langle r^2_{\rm ch}\rangle^{A'} - \langle r^2_{\rm ch}\rangle^{A}. \tag{15}$$

To assess odd-even staggering of charge radii and binding energies, we study three-point differences (either isotopic or isotonic):

$$\Delta^{(3)}_r(A) = \tfrac{1}{2}\left(r_{{\rm ch},A+1} - 2r_{{\rm ch},A} + r_{{\rm ch},A-1}\right), \tag{16}$$

$$\Delta^{(3)}_E(A) = \tfrac{1}{2}\left(E_{{\rm B},A+1} - 2E_{{\rm B},A} + E_{{\rm B},A-1}\right). \tag{17}$$

We shall also consider three-point binding energy differences involving ground states of even-even nuclei with

the same Z or N:

$$\Delta^{\rm ee}_E(A) = \tfrac{1}{2}\left(E_{{\rm B},A+2} - 2E_{{\rm B},A} + E_{{\rm B},A-2}\right). \quad (18)$$

For open-shell systems, $\Delta^{\rm ee}_E$ is proportional to the inverse of the pairing rotational moment of inertia, i.e., it is an excellent indicator of nucleonic pairing [39]. For the calibration of the spin-orbit functional, we also look at differences of single-particle energies, $\varepsilon_{\rm ls}$.

Nuclear matter properties (NMP) in symmetric homogeneous matter characterize the properties of a given functional. Here, in addition to the equilibrium density, $\rho_{\rm eq}$, and energy-per-nucleon of symmetric nuclear matter at the equilibrium, E/A, we will investigate the following NMP: incompressibility K and effective mass m^*/m characterizing the isoscalar response; and symmetry energy J, slope of symmetry energy L, and Thomas-Reiche-Kuhn sum-rule enhancement $\kappa_{\rm TRK}$ characterizing the isovector response, see Refs. [12, 24, 40] for definitions. The sum-rule enhancement $\kappa_{\rm TRK}$ is an alternative way to parametrize the isovector effective mass. Those NMP can be conveniently used to characterize results obtained under different optimization strategies.

F. Optimization strategies and variants

The free parameters of Fayans EDF need to be constrained by experiment. These parameters should be global in the sense that they should provide a reasonable description of finite nuclei and extended nucleonic matter [17]. The situation resembles the Skyrme EDF optimization strategy [9], where the least-squares method [41, 42] has become the most widely used approach, see, e.g., [12, 43–45]. Here, we are going to adopt this strategy for tuning Fayans EDF to the global set of data and to compare it with a Skyrme functional tuned in the same way. To that end, we define a global quality measure

$$\chi^2(\mathbf{p}) = \sum_{n\in{\rm Obs.}} \frac{(\mathcal{O}^{\rm th}_n(\mathbf{p}) - \mathcal{O}^{\rm exp}_n)^2}{\Delta^2\mathcal{O}_n}, \quad (19)$$

where the sum runs over all fit-observables $\mathcal{O}_n$, $\mathcal{O}^{\rm th}_n$ are predicted values, $\mathcal{O}^{\rm exp}_n$ are experimental values, and $\Delta\mathcal{O}_n$ are adopted errors chosen to regulate the relative weights of the different observables. The χ^2 is a function of the model parameters $\mathbf{p}$ through the parameter dependence of $\mathcal{O}^{\rm th}_n(\mathbf{p})$. The optimal parameter set $\mathbf{p}_0$ is the one which minimizes χ^2, i.e. $\mathcal{O}^{\rm th}_n(\mathbf{p}_0) \le \mathcal{O}^{\rm th}_n(\mathbf{p})$ for all $\mathbf{p}$.

To optimize Skyrme and Fayans functionals, we employed several datasets containing various combinations of fit-observables. They are listed in Table I, and the parametrizations resulting from different combinations of datasets are defined in Table II.

Having optimized the functionals, we use the resulting covariance matrices to carry out the correlation analysis as explained, e.g., in Refs. [45, 48, 49]. In particular, we employ a dimensionless product-moment correlation

TABLE I. The datasets used to constrain Skyrme and Fayans EDFs optimized in this work. The basic dataset of [24] including 224 experimental data points in total is considered in all cases; hence, it is not mentioned explicitly. For instance, the dataset $\Delta E^{\rm ee}$ includes the basic dataset in addition to the specific data listed below. The numbers in brackets (energies in MeV and radii in fm) indicate the adopted errors in χ^2 (19). The adopted errors for $\Delta E^{\rm oe}$ were chosen in accordance with the same choice for the spectral gaps in Ref. [24]. The adopted errors for $\Delta E^{\rm ee}$ were derived by estimating the effect of ground state correlations as in [46]. Experimental nuclear masses and charge radii were taken from Refs. [47] and [3], respectively.

Dataset	Fit-observables
basic:	dataset of SV-min [24]: $E_{\rm B}$, $R_{\rm diff}$ $r_{\rm ch}$, $\sigma_{\rm ch}$, $\varepsilon_{\rm ls}$
$\boldsymbol{\Delta E^{\rm oe}}$**:**	neutron $\Delta^{(3)}_E$ (17) in: ^{44}Ca (0.24), ^{44}Ca (0.36), ^{122}Sn (0.36), ^{124}Sn (0.36), ^{126}Sn (0.24), ^{128}Sn (0.24), ^{204}Pb (0.24), ^{206}Pb (0.36), ^{210}Pb (0.36); proton $\Delta^{(3)}_E$ (17) in: ^{86}Er (0.36), ^{88}Sr (0.24), ^{90}Zr (0.12), ^{92}Mo (0.24), ^{94}Ru (0.24), ^{136}Xe(0.24), ^{138}Ba (0.24), ^{140}Ce (0.24), ^{142}Nd (0.24), ^{144}Sm (0.24), ^{146}Gd (0.24), ^{148}Dy (0.24);
$\boldsymbol{\Delta E^{\rm ee}}$**:**	neutron $\Delta^{\rm ee}_E$ (18) in: ^{44}Ca (0.12), ^{118}Sn (0.36), ^{120}Sn (0.36), ^{122}Sn(0.13), ^{124}Sn(0.24); proton $\Delta^{\rm ee}_E$ (18) in: ^{36}Kr (0.36), ^{88}Sr (0.36), ^{90}Zr (0.24), ^{92}Mo (0.12), ^{94}Ru(0.24), ^{136}Xe (0.24), ^{138}Ba (0.24), ^{140}Ce (0.24), ^{142}Nd (0.24), ^{214}Ra (0.24), ^{216}Hg (0.24)
$\boldsymbol{\Delta r}$**:**	$\delta\langle r^2\rangle$ (15) for Ca isotopes: $\delta\langle r^2\rangle^{48,40}$ (0.008), $\delta\langle r^2\rangle^{48,44}$ (0.008), $\delta\langle r^2\rangle^{52,48}$ (0.02);
$\boldsymbol{\Delta r^{\rm oe}}$**:**	odd-even staggering: $\delta\langle r^2\rangle^{43,44}$(Ca) (0.002), $\delta\langle r^2\rangle^{119,120}$(Sn) (0.002).

TABLE II. Energy density functionals optimized in this work and the associated fit-observables as defined in Table I. The basic SV-min dataset of [24] is considered in all cases. All Fy functionals employ the Fayans functional of Sec. II C except for Fy($h^{\rm s}_\nabla$=0) and Fy(h^{ξ}_∇=0), in which the surface and pairing gradient terms are put to zero, respectively. Sk+PFy mixes the Skyrme functional in the particle-hole channel with the Fayans pairing functional (14) with $\gamma = 1$. In all cases, the c.m. correction is added.

EDF	$\Delta E^{\rm oe}$	Δr	$\Delta r^{\rm oe}$
Fy(std)	+	−	−
Fy(nogap)	−	−	−
Fy($\boldsymbol{\Delta r}$)	+	+	−
Fy($\boldsymbol{\Delta r, \Delta r^{\rm oe}}$)	+	+	+
Fy($\boldsymbol{h^{\xi}_\nabla}$=0)	+	+	−
Fy($\boldsymbol{h^{\rm s}_\nabla}$=0)	+	+	−
Sk+PFy	+	+	−
Sk+PFy(std)	+	−	−

coefficient [42]:

$$r_{AB} = \frac{|\overline{\Delta A\,\Delta B}|}{\sqrt{\overline{\Delta A^2}\;\overline{\Delta B^2}}}, \tag{20}$$

which measures the covariance between two observables A and B. A value $r_{AB} = 1$ means fully correlated, $r_{AB} = -1$ fully anti-correlated, and $r_{AB} = 0$ uncorrelated. In linear least squares regression, the square of the correlation coefficient r^2_{AB} is denoted the coefficient of determination. In our correlation analysis of functional parameters, we shall be inspecting matrices of r^2_{AB}.

G. Numerical considerations

In this work, pertaining to well-bound systems, we apply the HF+BCS approach rather than the full HFB; hence, the canonical wave functions are approximated by the HF orbitals and the related occupations are given by the standard BCS amplitudes. Spherical Hartree-Fock wave functions, densities, and mean-fields are represented on a 1D grid in spherical coordinates [50]. We use a grid spacing of 0.3 fm and 32–48 grid points depending on system size. The HF+BCS equations are solved with an accelerated gradient iteration technique [51].

We use the soft pairing cutoff [52] in BCS defined by the cutoff energy $\epsilon_{\rm cut} = 15\,$MeV with respect to the Fermi energy and the width $\Delta\epsilon = \epsilon_{\rm cut}/10$. Although seemingly straightforward, pairing raises a subtle problem around a phase transition between paired and normal state around closed shells, which may result in numerical instabilities. We avoid such unphysical behavior by using the stabilized pairing of [53] arranged to guarantee in smooth manner a minimal gap of $\Delta = 0.3\,$MeV, which is well below the typical pairing gap of 1–2 MeV; hence, it has negligible influence on nuclear bulk properties as binding energy and radii.

Odd-A nuclei are treated in the standard uniform filling approximation to blocking, in which a blocked nucleon is put with equal probability in each of the degenerate magnetic sub-states [18, 54]; hence, time-reversal symmetry is conserved. To find the ground state, we carry out blocked calculations for all shells near the Fermi energy and select the blocked state with lowest energy. It is to be noted that our spherical blocking calculations cannot account for multipole- and spin-polarization effects. Thus the experimental data in Table I on 3-point gaps $\Delta^{(3)}_E$ and $\Delta^{(3)}_r$ were selected in such a way that the impact of deformation-polarization, spin-polarization, and correlation effects is minimal. While these quantities can be affected by time-odd polarizations, the corresponding corrections are expected to be small [55, 56].

To find the optimal parameter set of parameters $\mathbf{p}_0$ we carry out multidimensional minimization of χ^2. Here we use two iterative strategies: a multi-dimensional method of determinants as outlined in Ref. [41], and succession of one-dimensional minimizations according to Powells method [57]. The first method is much faster and it has the great advantage to provide the full covariance matrix, which is needed for covariance analysis and error estimates [45, 49, 58, 59]. However, it easily gets stuck in conflicting situations where one or a few data points constitute a large faction of χ^2, as this often happens when trying to accommodate isotopic shifts. Here we switch to the Powell method which is comparably slow but unerringly drives χ^2 to a minimum. To acquire more confidence that the minimum found is global, we restart iterations several times by stochastically stirring up the model parameters $\mathbf{p}$.

III. RESULTS

A. Nuclear Matter Parameters

The volume term $\mathcal{E}^{\rm v}_{\rm Fy}$ of Fayans EDF determines its nuclear matter parameters. As a matter of fact, the volume term coupling constants of the original FaNDF^0 parametrization [17] were fixed by fitting them to the equation of state of symmetric infinite nuclear matter. Table III displays NMP of selected Fayans and Skyrme functionals used and optimized in this work. It is satisfying to see that the values of NMP in Table III are consistent (within error bars) with each other and with the range allowed by theory [40] and experiment/observations [60, 61]. The only notable exception is a relatively low mean value of L obtained in Sk+PFy. Considering that Sk+PFy and SV-min are based on the same particle-hole interaction parametrized to a very similar dataset, it is surprising to see an unexpectedly large impact of the additional data on differential charge radii on the symmetry energy slope. We checked that the Sk+PFy fit without a constrain on isotopic shift yields $L = 41\,$MeV, which is a typical value as in other parametrizations. We also remark that L is also sensitive to the density dependence of the pairing channel. By re-optimizing Sk+PFy with the pairing functional having different density dependence, $\gamma = 2/3$, we obtain $L = -3 \pm 17\,$MeV, which is unreasonably low. As seen in Fig. 1 below, such a low value of γ is disfavored by our optimization protocol.

B. Optimized Functionals

The parameters of EDFs used and optimized in this work are displayed in Tables IV (Fayans functionals) and V (Skyrme). The coupling constants characterizing the isoscalar part of the volume term (10) are similar between different Fayans functionals. This is not surprising in light of similarity of NMP in Table III. The parameters of the particle-hole interaction of Fy(Δr) and Fy($\Delta r, \Delta r^{\rm oe}$) are not far from the original FaNDF^0. This is not the case for the isovector-volume and surface terms

TABLE III. NMP of Fayans and Skyrme functionals used in this work.

NMP	FaNDF^0	Fy(std)	Fy(Δr)	Fy($\Delta r, \Delta r^{\rm oe}$)	SV-min	Sk+PFy
$\rho_{\rm eq}$ (fm^{-3})	0.160	0.163±0.002	0.160±0.002	0.161±0.001	0.162±0.001	0.163±0.001
E/A (MeV)	−16.00	−16.10±0.05	−16.11±0.04	−16.12±0.03	−15.91±0.04	−15.94±0.03
K (MeV)	219	219±15	219±12	220±18	222±7	229±5
J (MeV)	30	31±2	29±2	30±1	31±2	30±1
L (MeV)	30	59±22	30±24	35±21	45±26	18±18

TABLE IV. Parameters of the various Fayans functionals optimized in this work compared to the original FaNDF^0 parametrization. The parameters fitted in Fy(std), Fy(Δr), and Fy($\Delta r, \Delta r^{\rm oe}$) are displayed in the upper panel while the lower panel lists those that are fixed. The parameters are given with the number of digits as required for sufficient precision of the calculations. $\rho_{\rm sat}$ is in fm^{-3}; other parameters are dimensionless.

	FaNDF^0	Fy(std)	Fy(Δr)	Fy($\Delta r, \Delta r^{\rm oe}$)
$a_+^{\rm v}$	−9.559	−9.495922	−9.542989	−9.534242
$h_{1+}^{\rm v}$	0.633	0.6271056	0.6323225	0.6317662
$h_{2+}^{\rm v}$	0.131	0.1452334	0.1343786	0.1348917
$a_-^{\rm v}$	4.428	12.4741	4.18236	3.96619
$h_{1-}^{\rm v}$	0.250	−1.38754	0.253776	0.206941
$h_{2-}^{\rm v}$	1.300	19.3795	1.21502	1.16421
$a_+^{\rm s}$	0.600	0.5241615	0.6047266	0.5917059
$h_\nabla^{\rm s}$	0.440	0.0992	0.6656	0.4861
κ	0.19	0.189640	0.187922	0.197785
κ'	0.0	0.0250	−0.0237	−0.0052
$f_{\rm ex}^\xi$	−2.8	−1.636	−4.472	−4.265
h_+^ξ	2.8	1.130	4.229	3.9618
h_∇^ξ	2.2	0.013	3.227	3.8732
σ	1/3	1/3	1/3	1/3
$h_+^{\rm s}$	$h_{2+}^{\rm v}$	0	0	0
$h_{\rm Coul}$	0.941	0	0	0
$\rho_{\rm sat}$	0.160	0.160	0.160	0.160
$\rho_{\rm pair}$	$\rho_{\rm sat}$	$\rho_{\rm sat}$	$\rho_{\rm sat}$	$\rho_{\rm sat}$
γ	1	2/3	2/3	2/3

TABLE V. Parameters of the Skyrme functionals SV-min and Sky+PFy other than NMP shown in Table III: m^*/m and $\kappa_{\rm TRK}$ are dimensionless; $C_t^{\rho\Delta\rho}$ and $C_t^{\rho\nabla J}$ are in MeV fm^5; and $\rho_{\rm pair}$ is in fm^{-3}. The remaining pairing parameters of Sky+PFy are: $\rho_{\rm sat}$=0.16 fm^{-3}, γ = 1, $f_{\rm ex}^\xi$ = −3.3247 ± 0.31, h_+^ξ = 2.7952 ± 0.35, and h_∇^ξ = 4.8432 ± 0.70.

	SV-min	Sky+PFy
m^*/m	0.9518±0.07	1.0117±0.08
$\kappa_{\rm TRK}$	0.0765±0.28	0.1167±0.13
$C_0^{\rho\Delta\rho}$	−89.205±5.2	−23.499±6.5
$C_1^{\rho\Delta\rho}$	−35.377±39	25.734±17
$C_0^{\rho\nabla J}$	−101.581±4.9	−72.390±3.9
$C_1^{\rho\nabla J}$	−22.968±19	8.773±40
$\rho_{\rm pair}$	0.211591±0.05	0.16

of Fy(std). This suggests that constraining $\delta\langle r^2\rangle$ plays a key role for determining the spectroscopic quality of the Fayans model. Indeed, Table IV shows that the coupling constants $h_\nabla^{\rm s}$ and h_∇^ξ determining the strengths of the gradient terms $\propto (\nabla\rho_0)^2$ in the Fayans surface and pairing functional, respectively, are increased by orders of magnitude when the data on differential radii are added to the dataset. Another interesting outcome is the significant difference between the parameters of SV-min and Sk+PFy shown in Table V, again primarily attributed to the additional data on differential radii used to constrain Sk+PFy. It is worth noting that the value of h_∇^ξ of Sk+PFy is in the same range that that of Fy(Δr).

The parameter γ entering the density dependence of the Fayans pairing functional is of particular interest as it changes the character of pairing potential from surface-type ($\gamma < 1, \rho_{\rm pair} \leq \rho_{\rm sat}$) to mixed-type ($\gamma \geq 1, \rho_{\rm pair} > \rho_{\rm sat}$). Figure 1(a) shows the dependence of the quality measure (19) on γ. The parametrization Fy(std) is fairly insensitive to γ as the value of h_+^ξ is significantly reduced for this parametrization as compared to the other ones in Fig. 1. The constraint on differential radii in Fy(Δr) clearly favors γ = 2/3. This is due to the interplay between the surface-gradient effect and pairing term of the Fayans functional. Indeed, eliminating the surface-gradient correction in Fy($h_\nabla^{\rm s}$=0) tends to favor larger values of γ, and this is in line with the Sk+PFy result. To illustrate the impact of γ and the data on differential radii on odd-even binding energy staggering, Fig. 1(b) shows $\Delta_E^{(3)}$ in ^{204}Pb. The prediction of Fy(std) is close to experiment and hardly varies with γ. It is seen that the additional dataset Δr does impact pairing correlations significantly, and – by increasing h_+^ξ – it gives rise to large variations of $\Delta_E^{(3)}$ with γ.

C. Global performance

Figure 2 illustrates the performance of Fayans and Skyrme parametrizations used/optimized in this work. The optimization quality is measured in terms of average and r.m.s. deviations of fit observables from experiment:

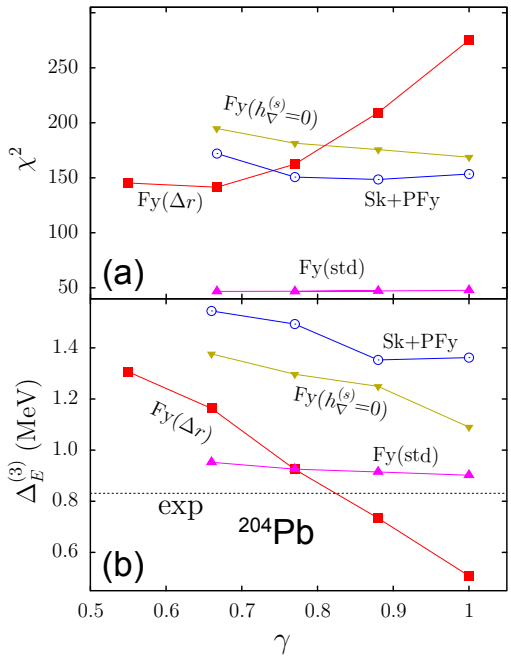

FIG. 1. Quality measure χ^2 (top) and odd-even binding-energy staggering $\Delta_E^{(3)}$ for ^{204}Pb (bottom) and as functions of the γ parameter of the Fayans pairing functional for Fy(std), Fy(Δr), Fy(h_∇^s), and Sk+PFy.

$$\overline{\mathcal{D}}_\mathcal{O} = \frac{\sum_n \left(\mathcal{O}_n^{\rm th} - \mathcal{O}_n^{\rm exp}\right)}{N_{\rm data}}, \tag{21a}$$

$$\overline{\Delta\mathcal{D}}_\mathcal{O} = \sqrt{\frac{\sum_n \left(\mathcal{O}_n^{\rm th} - \mathcal{O}^{\rm exp}\right)^2}{N_{\rm data}} - \overline{\mathcal{D}}_\mathcal{O}^2}, \tag{21b}$$

where $\mathcal{O}$ stands for one of the observables: $E_{\rm B}, \Delta_E^{(3)}$, and charge form factor characteristics: $R_{\rm diff}$, $\sigma_{\rm ch}$, and $r_{\rm ch}$. The parametrizations Fy(std), Fy(nogap), and SV-min, optimized to similar datasets yield results of comparable quality for bulk observables (energies and charge form factor characteristics). This performance deteriorates as the data on Δr and $\Delta r^{\rm oe}$ are added to the dataset. This is seen in large error bars on the values of $E_{\rm B}$, $\Delta_E^{(3)}$, $R_{\rm diff}$, $\sigma_{\rm ch}$, and $r_{\rm ch}$ predicted by Fy(Δr) and Fy($\Delta r, \Delta r^{\rm oe}$).

Differential radii for the Ca isotopes are are shown in Fig. 2(d). One can see that by constraining the functional by additional Δr data, as done for Fy(Δr), Fy($\Delta r, \Delta r^{\rm oe}$), and Sk+PFy, one is able to reproduce experiment for A = 40 and 44. The unexpectedly large charge radius in ^{52}Ca [6] is reproduced by the Δr-constrained Fayans functionals but it is underestimated in Sk+PFy and also in Fy(std), Fy(nogap), and SV-min.

Interestingly, the odd-even energy staggering $\Delta_E^{(3)}$ in Ca is reproduced reasonably well by all models, see Figs. 2(b) and (f). When looking into details, however, one can see that by adding data on $\Delta_E^{(3)}$ to the basic dataset, helps reducing theoretical error when going from Fy(nogap) to Fy(std).

As pointed out in Ref. [18, 20], the odd-even staggering of charge radii can be attributed to the contribution to the mean-field potential arising from the pairing interaction (14):

$$h_{\rm pair} = \tfrac{2\varepsilon_F}{3\rho_{\rm sat}} \Big\{ h_+^\xi \gamma x_0^{\gamma-1} (\breve{\rho}_n^2 + \breve{\rho}_p^2) \tag{22a}$$

$$-2h_\nabla^\xi r_s^2 \nabla \left[(\breve{\rho}_n^2 + \breve{\rho}_p^2) \nabla x_0 \right] \Big\}, \tag{22b}$$

where we explicitly put $x_{\rm pair} = x_0$ (as $\rho_{\rm pair} = \rho_{\rm sat}$). The field (22) produces a direct coupling between the isoscalar particle density ρ_0 and pairing densities $\breve{\rho}_n$ and $\breve{\rho}_p$, which results in the odd-even staggering in charge radii. Indeed, the blocking effect in an odd-A nucleus yields a reduced pairing density $\breve{\rho}_n$, which in turn impacts the proton (or charge) density, hence $r_{\rm ch}$. Figure 2(e) illustrates the importance of the couplings (22) for the Ca chain. The parametrizations Fy(std), Fy(nogap), and SV-min dramatically underestimate the magnitude of $\Delta_r^{(3)}$. Indeed, in these models the coupling constant h_∇^ξ is either zero (SV-min) or very small (Fy(std) and Fy(nogap)), and $\Delta_r^{(3)}$ is driven by the first term (22a). In other models, having large values of h_∇^ξ, the staggering primarily results from the second term (22b). Here we see that the additional information contained in datasets Δr and $\Delta r^{\rm oe}$ is absolutely crucial for boosting h_∇^ξ.

To check the importance of c.m. correction, we carried out two sets of calculations for the observables shown in Fig. 2: with and without c.m. correction. We conclude that the impact of the c.m. term is negligible for radial properties, and plays fairly minor role for energies. In the following, we stick to calculations with the c.m. term added, but its effect is should be viewed as secondary.

The performance of optimized functionals with respect to $\Delta_E^{\rm ee}$ in ^{44}Ca, ^{124}Sn, ^{204}Pb, and ^{212}Pb is illustrated in Fig. 3. Since the Fayans pairing functional exhibits an A-dependent scaling, in order to include FaNDF^0 results in the mix, we scaled the parameters of FaNDF^0 pairing functional given in Table IV by an overall factor 1.2, which yields reasonable results for all nuclei in the sample considered. It is seen that for ^{44}Ca, ^{124}Sn, and ^{204}Pb, there is a great consistency between different functionals employed. Indeed, most information on pairing correlations is contained in the mass surface of even-even nuclei [39], and all our functionals shown in Fig. 3 utilize masses from the basic dataset of SV-min. The discrepancy between calculated and experimental values of $\Delta_E^{\rm ee}$ was discussed in Ref. [39]: the static pairing in ^{42,46}Ca is close to the unphysical pairing phase transition. For ^{212}Pb, the spread of predicted values of $\Delta_E^{\rm ee}$ is significant, with Fy(std) and Sk+PFy functionals overestimating pairing correlations significantly.

Figure 4 shows predicted differential radii $\delta\langle r^2\rangle^{48,A}$ for the Ca chain. The functionals optimized to the basic dataset, Fy(std) and SV-min, exhibit characteristic monotonic dependence on A [8], and the odd-even affect is almost nonexistent. As discussed earlier, the latter ef-

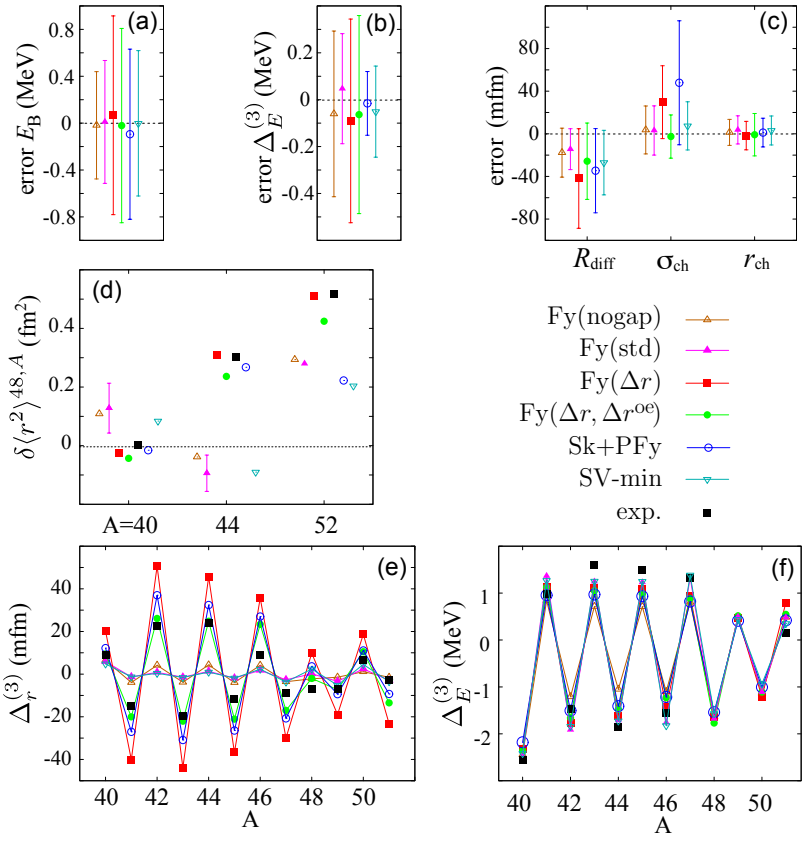

FIG. 2. Summary of global performance of Fayans and Skyrme parametrizations used/optimized in this work; for naming convention see Sec. II F. Top: average and r.m.s. deviations (21) for selected observables of the fit. Middle: Differential charge radii in Ca. Bottom: odd-even staggering of charge radii and binding energies in Ca isotopes.

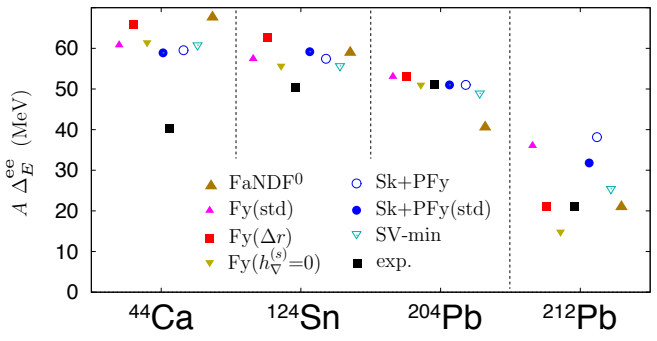

FIG. 3. Three-point binding energy difference Δ_E^{ee} (multiplied by the mass number to easily compare different systems) for the spherical open-shell nuclei ^{44}Ca, ^{124}Sn, ^{204}Pb, and ^{212}Pb computed with selected Fayans and Skyrme functionals and compared to experiment.

fect can be attributed to h_∇^ξ. The Fayans parametrization without the pairing gradient term Fy(h_∇^ξ=0) does not perform well either; while the magnitude of the odd-even staggering is slightly increased, the overall trend between ^{40}Ca and ^{48}Ca is incorrect. It is only in the functionals with the full Fayans pairing and constraints on differential radii that large $\Delta_r^{(3)}$ values can be obtained.

Another set of radius differences, which had raised much attention in the past is that along the Pb chain. It has been argued in [18, 31] that the Fayans pairing functional allows to reproduce the kink in $\delta\langle r^2\rangle$ at ^{208}Pb. In this case, however, pairing seems not to be the only influential agent. For instance, relativistic and Skyrme mean-field models can associate the kink with spin-orbit coupling [62, 63]. As it is a task of its own to disentangle various influences on the kink in ^{208}Pb, we are not addressing this observable here.

The functionals with the full Fayans pairing, namely Fy(Δr), Fy($\Delta r, \Delta r^{oe}$), and Sk+PFy, perform well up to ^{48}Ca. However, the $\delta\langle r^2\rangle$ values in $^{49-52}$Ca are underestimated in all models except for Fy(Δr). This seems to suggest that correlations beyond mean field [6, 8, 37] can play a role there. It is also interesting to note that the attempt to tune $\Delta_r^{(3)}$ in Fy($\Delta r, \Delta r^{oe}$) results in a deterioration of the reproduction of differential radii Δr.

To illustrate the performance of our optimized functionals for odd-even staggering in medium-mass and heavy nuclei, shown in Fig. 5 are their predictions for neutron values of $\Delta_r^{(3)}$ and $\Delta_E^{(3)}$ in ^{44}Ca, ^{64}Ni, ^{124}Sn, and ^{204}Pb. In accordance with the discussion around

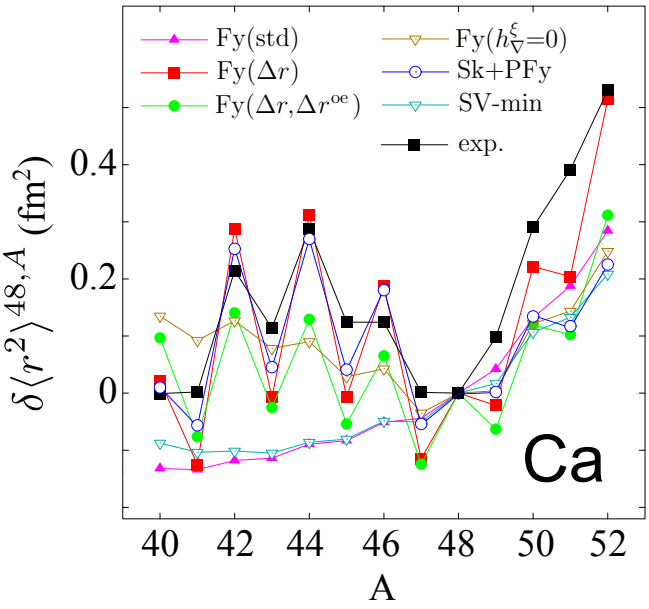

FIG. 4. Differential charge radii $\delta\langle r^2\rangle^{48,A}$ (15) in Ca predicted by Fayans and Skyrme parametrizations as indicated, and compared to experiment.

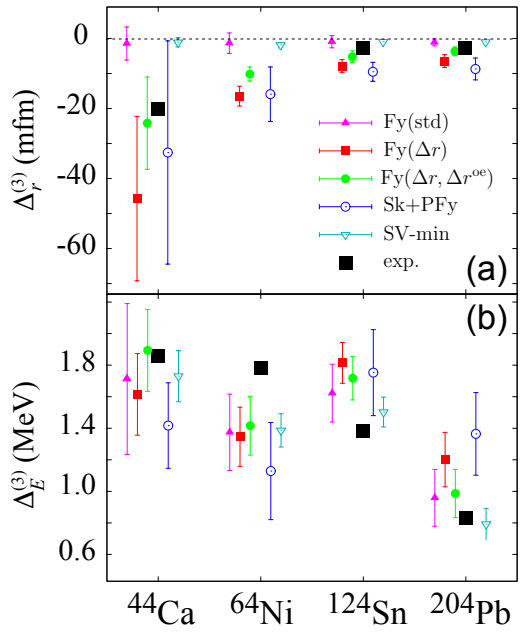

FIG. 5. Predicted mean values and variances of three-point neutron differences $\Delta_r^{(3)}$ (top) and $\Delta_E^{(3)}$ (bottom) in ^{44}Ca, ^{64}Ni, ^{124}Sn, and ^{204}Pb, predicted by selected Fayans and Skyrme functionals, and compared to experiment.

Fig. 4, Fy(std) and SV-min fail in reproducing $\Delta_r^{(3)}$, and Fy($\Delta r, \Delta r^{\rm oe}$) and Sk+PFy have a comparable performance. The results for $\Delta_E^{(3)}$ in ^{44}Ca, ^{64}Ni, and ^{124}Sn are consistent across different functionals. A large difference between experiment and Fy(Δr) and Sk+PFy results for ^{204}Pb has been puzzling. To explain this dramatic enhancement of pairing predicted by these models, in Fig. 6 we show the neutron pairing density $\breve{\rho}_n$ in ^{44}Ca, ^{124}Sn, ^{204}Pb, and ^{214}U obtained in different parametrizations. (^{214}U is slightly deformed in its ground state. However, for the purpose of this discussion, we considered it spherical.) In general, the shape of $\breve{\rho}_n$ is predicted consistently by all functionals considered. What is different is the overall magnitude of pairing density. In particular, in heavy nuclei such as ^{204}Pb and ^{214}U, $\breve{\rho}_n$ predicted by Sk+PFy and Fy(Δr) becomes very large, and this results in unreasonably large pairing fields. This is indicative of somehow uncontrolled A-dependence of Fayans pairing functional and explains previous results of Ref. [18], where it was necessary to increase the strength of pairing functional by as much as 35% when going from Pb to Ca.

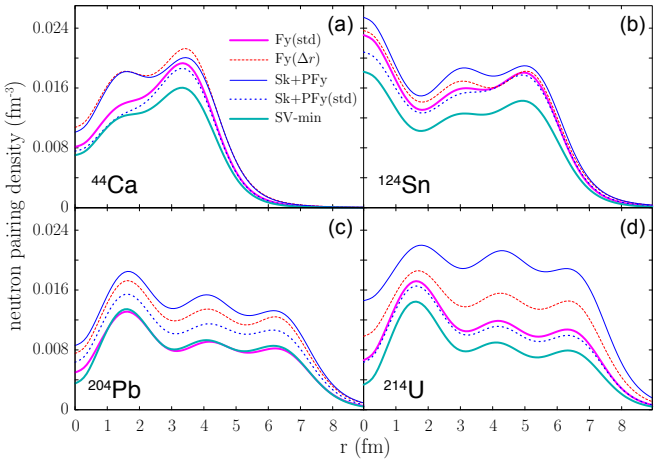

FIG. 6. Neutron pairing densities $\breve{\rho}_n$ in spherical configurations of ^{44}Ca, ^{124}Sn, ^{204}Pb, and ^{214}U, predicted by selected Fayans and Skyrme functionals.

Figure 7 compares proton HF potentials of Fy(std) and Fy(Δr) for ^{44}Ca and ^{48}Ca. Both FaNDF^0 and Fy(Δr) produce proton potentials with pronounced flattening, or even small pockets, in the surface region. Compared to Fy(std), this feature can be attributed to the large parameters $h_\nabla^{\rm s}$ and h_∇^ξ, which define the strength of gradient terms. It is instructive to see how these terms influence surface properties of the charge form factor. To this end, in Fig. 8 we show the isotopic trends of charge radii, diffraction radii, and surface thickness predicted with Fy(std), Fy(Δr), and FaNDF^0 along the Ca chain. These three quantities are related via [38, 64, 65]

$$r_{\rm ch} \approx \sqrt{\frac{3}{5}}\sqrt{R_{\rm diff}^2 + 5\sigma_{\rm ch}^2}. \tag{23}$$

The impact of the additional data on differential radii in Fy(Δr) is significant; the presence of this additional constraint results in a considerable reduction of $\sigma_{\rm ch}$ and a simultaneous increase of $R_{\rm diff}$. As a consequence, the

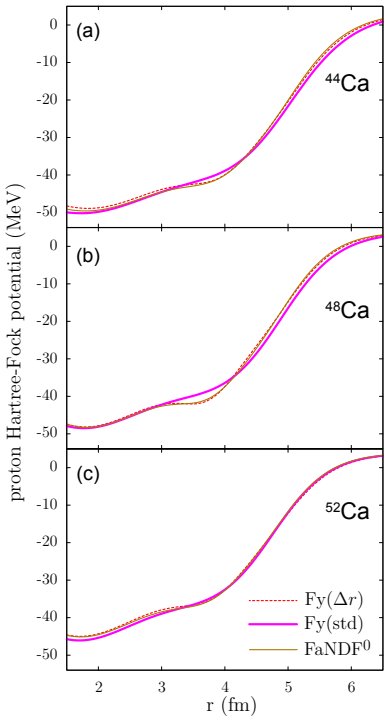

FIG. 7. Proton HF potential for ^{44}Ca (top), ^{48}Ca (middle) and ^{52}Ca (bottom) obtained in Fy(std), Fy(Δr), and FaNDF^0.

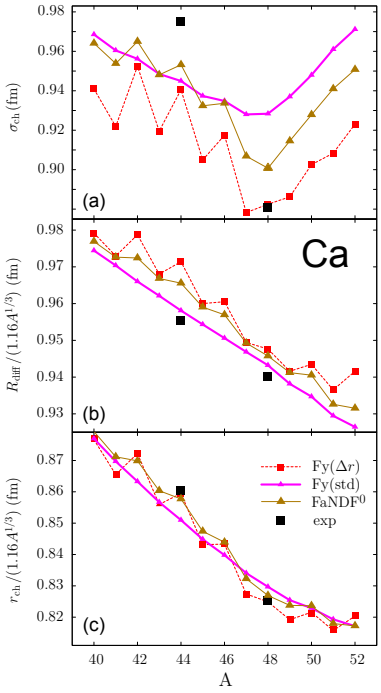

FIG. 8. Charge form factor characteristics, $\sigma_{\rm ch}$, $R_{\rm diff}$, and $r_{\rm ch}$, along the chain of Ca isotopes for Fy(std), Fy(Δr), and FaNDF^0. Experimental data are taken from Ref. [38].

charge radius of ^{44}Ca is increased, and that of ^{48}Ca is reduced, with respect to the Fy(std) prediction. While the properties of the charge form factor of ^{48}Ca are well reproduced by Fy(Δr), this is not the case for of ^{44}Ca, where a good agreement for $r_{\rm ch}$ is obtained at the cost of underestimating $\sigma_{\rm ch}$ and overestimating of $R_{\rm diff}$. Another interesting lesson offered by Fig. 8 is that the odd-even staggering of charge radii in Fy(Δr) and FaNDF^0 comes from an appreciable odd-even effect in $\sigma_{\rm ch}$ and $R_{\rm diff}$: both quantities are reduced in odd-A isotopes as compared to their even-even neighbors. This effect is virtually nonexistent in Fy(std), which again highlights the impact of large density gradient terms in Fy(Δr).

D. Correlations

To understand better the impact of individual parameters of the Fayans functional on calculated observables, in Fig. 9 we show the coefficients of determination r^2_{AB} for Fy(nogap) and Fy(Δr). Since Fy(nogap) has not been constrained to differential radii, it is particularly suitable for the analysis of correlations related to $\Delta^{(3)}_r$ and $\delta\langle r^2\rangle$.

That the odd-even staggering in charge radii is primarily driven by the pairing functional (14) is shown by the large values of r^2_{AB} between $\Delta^{(3)}_r$ and $f^{\xi}_{\rm ex}, h^{\xi}_{+}$, and h^{ξ}_{∇}. The key value of $\delta\langle r^2\rangle^{48,40}$(Ca) is primarily determined by the surface-energy coupling constants $a^{\rm s}_{+}$ and $h^{\rm s}_{\nabla}$. For Fy(Δr), correlations between $\delta\langle r^2\rangle$ values and surface-energy parameters are gone, as the differential radii in Ca we constrained in the fit. Adding the dataset Δr increases the impact of the pairing gradient term h^{ξ}_{∇} on charge radii and $\Delta^{(3)}_E$. For both functionals, spin-orbit parameters $C^{\rho\nabla J}_t$ correlate with neither charge radii nor pairing.

The matrices of r^2_{AB} for the Skyrme functionals SV-min and Sk-PFy are displayed in Fig. 10. As SV-min and Fy(nogap), and Sk+PFy and Fy(Δr) have been optimized to the same respective datasets, it is instructive to compare the corresponding coefficients of determination. In general, there is a good correspondence. In particular, for both Skyrme functionals, the correlations of $\delta\langle r^2\rangle$, $\Delta^{(3)}_r$, and $\Delta^{(3)}_E$ with pairing parameters are significant, this even more so as they employ different pairing models. Interestingly, we find marginal correlations between differential radii and parameters $C^{\rho\Delta\rho}_t$, $C^{\rho\nabla J}_t$, and $C^{\rho\tau}_t$ (not shown). This suggests that the impact of the surface energy on $\delta\langle r^2\rangle$ is less pronounced in the Skyrme case.

IV. CONCLUSIONS

By using the tools of numerical optimization and linear regression, we studied properties of the Fayans energy density functional FaNDF^0, which is known to provide superb description of selected nuclear properties, such as

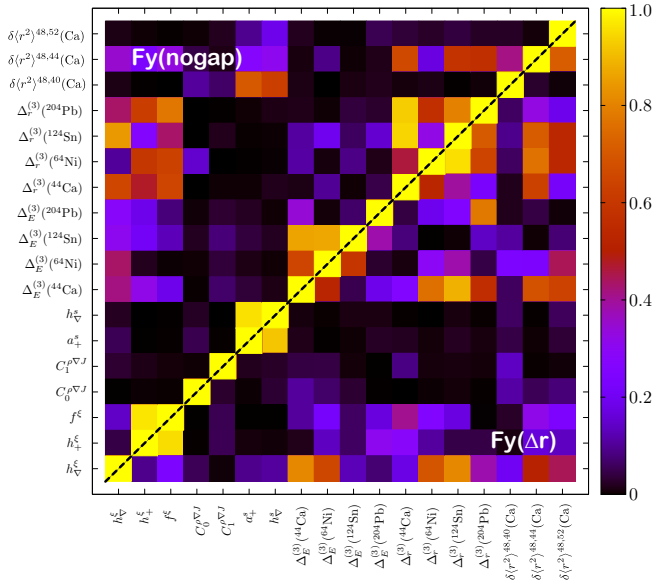

FIG. 9. Matrices of coefficients of determination r^2_{AB} for a selection of observables computed with the Fayans functionals Fy(nogap) (upper triangle) and Fy(Δr) (lower triangle).

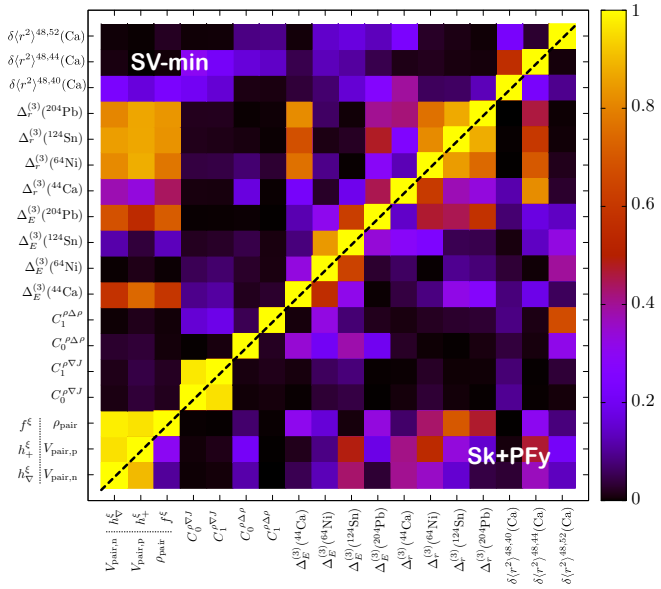

FIG. 10. Similar as in Fig. 9 except for the Skyrme parametrizations SV-min (upper triangle) and Sk-PFy (lower triangle).

charge radii and separation energies, and nuclear matter. By carefully selecting datasets of experimental data used in optimization, we generated functionals aimed to probe questions pertaining to different observables. The main conclusions of our study can be summarized as follows.

The pairing gradient term, controlled by the coupling constant h^{ξ}_{∇}, is arguably the most important ingredient in the Fayans functional. Without this term, it is impossible to reproduce the odd-even staggering $\Delta^{(3)}_r$ of charge radii and reproduce the intricate pattern of $r_{\rm ch}$ in the Ca chain. We note that by adding the Fayans pairing functional to the standard Skyrme functional, the resulting parametrization Sk+PFy, provides a comparable reproduction of the data as Fy(Δr). The large value of $\delta\langle r^2\rangle^{52,48}$(Ca) [6], while explained by Fy(Δr), still remains a puzzle as other Fayans functionals and Sk+PFy significantly underestimate experimental value.

The surface gradient term controlled by the coupling constant $h^{\rm s}_{\nabla}$ is less influential. While it is driving the near-zero value of $\delta\langle r^2\rangle^{40,48}$(Ca), it does not seem to be crucial for other radius differences. Moreover, the gradient terms of the Fayans model significantly change the surface behavior of the proton potential, as seen in Fig. 7 for FaNDF^0 and Fy(Δr).

The data on $\delta\langle r^2\rangle$ and $\Delta^{(3)}_r$ are important for characterizing the pairing functional. Our study demonstrates that the coupling constants $h^{\rm s}_{\nabla}$ and h^{ξ}_{∇} determining the strengths of the gradient terms are increased by orders of magnitude when the data on differential radii are added to the pool of fit-observables. In particular, the correlation analysis indicates that the radius staggering $\Delta^{(3)}_r$ is more sensitive to pairing than the energy staggering $\Delta^{(3)}_E$. Since the nuclear pairing functional is rather poorly constrained by experimental binding-energy differences alone, this has practically eliminated more sophisticated models of pairing EDF [23, 66]. In this respect, new-quality data on differential radii can help to calibrate a properly generalized pairing functional.

By comparing the Fy(std) results with those obtained with with the Fayans functional optimized to the basic+$\Delta E^{\rm ee}$ dataset (employing even-even energy differences instead of odd-even staggering), we find that the data on even-even binding energy differences $\Delta^{\rm ee}_E$ in open-shell nuclei carry very similar information content with respect to pairing as $\Delta^{(3)}_E$, while the interpretation of $\Delta^{\rm ee}_E$ in terms of pairing correlations is more straightforward. It is thus recommended that selected data on $\delta\langle r^2\rangle$, $\Delta^{(3)}_r$, and $\Delta^{\rm ee}_E$ are used in the future functional optimizations.

The analysis presented in this paper should be viewed as a useful starting point for future investigations. While the Fayans pairing functional has several attractive features, especially in the context of odd-even effect on charge radii, it fails short to reach the global description of pairing effects across the nuclear landscape. In particular, the parameters $f^{\xi}_{\rm ex}, h^{\xi}_{+}$, and h^{ξ}_{∇}, which provide excellent description of charge radii and pairing in spherical nuclei up to tin, dramatically overestimate pairing correlations around lead and in the actinides. This is consistent with the findings of Ref. [18], where an ad-hoc renormalization of pairing functional was imposed to provide agreement with experiment. Consequently, extensions of the current Fayans pairing functional should be investigated. The current Fayans pairing functional is manifestly isoscalar. However, as the Coulomb term does affect pairing, many Skyrme parametrizations such as SV-min employ isovector pairing functionals, see Ref. [27]

and references quoted therein. The definition (14) can easily be extended to accommodate the isovector dependence.

Extensions of the FaNDF^0 surface term (11) are also possible. By enlarging the experimental dataset, the parameter $h_+^{\rm s}$ could perhaps be pinned down with an acceptable accuracy. Moreover, the dependence of $\mathcal{E}_{\rm Fy}^{\rm s}$ on the isovector density x_1 should be considered, as the current parametrization cannot account for the surface-symmetry effects. Another strategy worth exploring is to replace the surface term (11) by the folded DF3 expression [15, 29, 30].

The extension of the functional FaNDF^0 to deformed nuclei [28], augmented by Fayans pairing, will allow the global optimization of the extended Fayans and Sk+PFy models to diverse data on spherical and deformed nuclei, at the full deformed HFB level, using the well-tested UNEDF methodology [12, 34, 67]. Work along these lines is in progress.

ACKNOWLEDGMENTS

We thank E.E. Saperstein and S.V. Tolokonnikov for their invaluable help in explaining the subtilities of the Fayans functional. This material is based upon work supported by the U.S. Department of Energy, Office of Science, Office of Nuclear Physics under award numbers DE-SC0013365 (Michigan State University) and DE-SC0008511 (NUCLEI SciDAC-3 collaboration).

[1] G. Hagen, A. Ekström, C. Forssén, G. R. Jansen, W. Nazarewicz, T. Papenbrock, K. A. Wendt, S. Bacca, N. Barnea, B. Carlsson, C. Drischler, K. Hebeler, M. Hjorth-Jensen, M. Miorelli, G. Orlandini, A. Schwenk, and J. Simonis, Nat. Phys. **12**, 186 (2016).
[2] P.-G. Reinhard and W. Nazarewicz, Phys. Rev. C **93**, 051303 (May 2016).
[3] I. Angeli and K. P. Marinova, At. Data Nucl. Data Tables **99**, 69 (2013).
[4] B. H. Sun, C. Y. Liu, and H. X. Wang, Phys. Rev. C **95**, 014307 (Jan 2017).
[5] H. De Witte *et al.*, Phys. Rev. Lett. **98**, 112502 (Mar 2007).
[6] F. R. Garcia Ruiz *et al.*, Nat. Phys. **12**, 594 (2016).
[7] D. M. Rossi *et al.*, Phys. Rev. C **92**, 014305 (Jul 2015).
[8] K. Minamisono *et al.*, Phys. Rev. Lett. **117**, 252501 (Dec 2016).
[9] M. Bender, P.-H. Heenen, and P.-G. Reinhard, Rev. Mod. Phys. **75**, 121 (Jan 2003).
[10] Z. Patyk, A. Baran, J. F. Berger, J. Dechargé, J. Dobaczewski, P. Ring, and A. Sobiczewski, Phys. Rev. C **59**, 704 (Feb 1999).
[11] S. Goriely, S. Hilaire, M. Girod, and S. Péru, Phys. Rev. Lett. **102**, 242501 (Jun 2009).
[12] M. Kortelainen, T. Lesinski, J. Moré, W. Nazarewicz, J. Sarich, N. Schunck, M. V. Stoitsov, and S. Wild, Phys. Rev. C **82**, 024313 (Aug 2010).
[13] R. Utama, W.-C. Chen, and J. Piekarewicz, J. Phys. G **43**, 114002 (2016).
[14] A. V. Smirnov, S. V. Tolokonnikov, and S. A. Fayans, Sov. J. Nucl. Phys. **48**, 995 (1988).
[15] S. Fayans, E. Trykov, and D. Zawischa, Nucl. Phys. A **568**, 523 (1994).
[16] I. N. Borzov, S. A. Fayans, E. Krömer, and D. Zawischa, Z. Phys. A **355**, 117 (1996).
[17] S. A. Fayans, JETP Lett. **68**, 169 (1998).
[18] S. Fayans, S. Tolokonnikov, E. Trykov, and D. Zawischa, Nucl. Phys. A **676**, 49 (2000).
[19] S. Fayans, S. Tolokonnikov, E. Trykov, and D. Zawischa, Phys. Lett. B **338**, 1 (1994).
[20] S. Fayans and D. Zawischa, Phys. Lett. B **383**, 19 (1996).
[21] Y. Yu and A. Bulgac, arXiv:nucl-th/0302007(2003).
[22] Y. M. Engel, D. M. Brink, K. Goeke, S. J. Krieger, and D. Vautherin, Nucl. Phys. A **249**, 215 (1975).
[23] E. Perlińska, S. G. Rohoziński, J. Dobaczewski, and W. Nazarewicz, Phys. Rev. C **69**, 014316 (Jan 2004).
[24] P. Klüpfel, P.-G. Reinhard, T. J. Bürvenich, and J. A. Maruhn, Phys. Rev. C **79**, 034310 (Mar 2009).
[25] J. Dobaczewski, W. Nazarewicz, and P.-G. Reinhard, Nucl. Phys. A **693**, 361 (2001).
[26] J. Dobaczewski, W. Nazarewicz, and M. V. Stoitsov, Eur. Phys. J. A **15**, 21 (2002).
[27] G. F. Bertsch, C. A. Bertulani, W. Nazarewicz, N. Schunck, and M. V. Stoitsov, Phys. Rev. C **79**, 034306 (Mar 2009).
[28] S. V. Tolokonnikov, I. N. Borzov, M. Kortelainen, Y. S. Lutostansky, and E. E. Saperstein, J. Phys. G **42**, 075102 (2015).
[29] E. Krömer, S. Tolokonnikov, S. Fayans, and D. Zawischa, Phys. Lett. B **363**, 12 (1995).
[30] D. Horen, G. Satchler, S. Fayans, and E. Trykov, Nucl. Phys. A **600**, 193 (1996).
[31] S. V. Tolokonnikov and E. E. Saperstein, Phys. At. Nucl. **73**, 1684 (2010).
[32] J. Erler, P. Klüpfel, and P.-G. Reinhard, Phys. Rev. C **82**, 044307 (2010).
[33] T. Lesinski, M. Bender, K. Bennaceur, T. Duguet, and J. Meyer, Phys. Rev. C **76**, 014312 (2007).
[34] M. Kortelainen, J. McDonnell, W. Nazarewicz, E. Olsen, P.-G. Reinhard, J. Sarich, N. Schunck, S. M. Wild, D. Davesne, J. Erler, and A. Pastore, Phys. Rev. C **89**, 054314 (2014).
[35] W. Kim, J. P. Connelly, J. H. Heisenberg, F. W. Hersman, T. E. Milliman, J. E. Wise, C. N. Papanicolas, S. A. Fayans, and A. P. Platonov, Phys. Rev. C **46**, 1656 (Nov 1992).
[36] N. V. Gnezdilov, I. N. Borzov, E. E. Saperstein, and S. V. Tolokonnikov, Phys. Rev. C **89**, 034304 (2014).
[37] E. E. Saperstein, I. N. Borzov, and S. V. Tolokonnikov, JETP Letters **104**, 218 (2016).
[38] J. Friedrich and N. Vögler, Nucl. Phys. A **373**, 192 (1982).
[39] N. Hinohara and W. Nazarewicz, Phys. Rev. Lett. **116**, 152502 (Apr 2016).

[40] W. Nazarewicz, P.-G. Reinhard, W. Satuła, and D. Vretenar, Eur. Phys. J. A **50**, 20 (2014).

[41] P. R. Bevington and D. K. Robinson, *Data Reduction and Error Analysis for the Physical Sciences* (McGraw-Hill, 2003).

[42] S. Brandt, *Statistical and computational methods in data analysis* (Springer-Verlag, New York, 1997).

[43] J. Friedrich and P.-G. Reinhard, Phys. Rev. C **33**, 335 (1986).

[44] M. Samyn, S. Goriely, P.-H. Heenen, J. M. Pearson, and F. Tondeur, Nucl. Phys. A **700**, 142 (2002).

[45] J. Dobaczewski, W. Nazarewicz, and P.-G. Reinhard, J. Phys. G **41**, 074001 (2014).

[46] P. Klüpfel, J. Erler, P.-G. Reinhard, and J. A. Maruhn, Eur. Phys. J. A **37**, 343 (2008).

[47] G. Audi, F. Kondev, M. Wang, W. Huang, and S. Naimi, Chin. Phys. C **41**, 030001 (2017).

[48] P.-G. Reinhard and W. Nazarewicz, Phys. Rev. C **81**, 051303(R) (May 2010).

[49] J. Erler and P.-G. Reinhard, J. Phys. G **42**, 034026 (2015).

[50] P.-G. Reinhard, in *Computational Nuclear Physics I - Nuclear Structure*, edited by K. Langanke, S. Koonin, and J. Maruhn (Springer, Berlin, 1991) p. 28.

[51] P.-G. Reinhard and R. Cusson, Nucl. Phys. A **378**, 418 (1982).

[52] S. J. Krieger, P. Bonche, H. Flocard, P. Quentin, and M. S. Weiss, Nucl. Phys. A **517**, 275 (1990).

[53] J. Erler, P. Klüpfel, and P.-G. Reinhard, Eur. Phys. J. A **37**, 81 (2008).

[54] T. Duguet, P. Bonche, P.-H. Heenen, and J. Meyer, Phys. Rev. C **65**, 014310 (Dec 2001).

[55] N. Schunck, J. Dobaczewski, J. McDonnell, J. Moré, W. Nazarewicz, J. Sarich, and M. V. Stoitsov, Phys. Rev. C **81**, 024316 (2010).

[56] K. J. Pototzky, J. Erler, P.-G. Reinhard, and V. O. Nesterenko, Eur. Phys. J. A **46**, 299 (2010).

[57] W. H. Press, S. A. Teukolsky, W. T. Vetterling, and B. P. Flannery, *Numerical Recipes in C: The Art of Scientific Computing*, 2nd ed. (Cambridge University Press, New York, 1992).

[58] P.-G. Reinhard and W. Nazarewicz, Phys. Rev. C **87**, 014324 (2013).

[59] T. Haverinen and M. Kortelainen, J. Phys. G **44**, 044008 (2017).

[60] J. M. Lattimer and A. W. Steiner, Eur. Phys. J. A **50**, 40 (2014).

[61] M. Oertel, M. Hempel, T. Klähn, and S. Typel, Rev. Mod. Phys. **89**, 015007 (Mar 2017).

[62] M. M. Sharma, G. A. Lalazissis, and P. Ring, Phys. Lett. B **317**, 9 (1993).

[63] P.-G. Reinhard and H. Flocard, Nucl. Phys. A **584**, 467 (1995).

[64] R. H. Helm, Phys. Rev. **104**, 1466 (Dec 1956).

[65] S. Mizutori, J. Dobaczewski, G. A. Lalazissis, W. Nazarewicz, and P.-G. Reinhard, Phys. Rev. C **61**, 044326 (Mar 2000).

[66] M. Yamagami, J. Margueron, H. Sagawa, and K. Hagino, Phys. Rev. C **86**, 034333 (Sep 2012).

[67] M. Kortelainen, J. McDonnell, W. Nazarewicz, P.-G. Reinhard, J. Sarich, N. Schunck, M. V. Stoitsov, and S. M. Wild, Phys. Rev. C **85**, 024304 (2012).